A simple two-step approach to the fabrication of VO_2-based coatings with unique thermochromic features for energy-efficient smart glazing

A. J. Santos[a,b,c,*], N. Martin[c], J. Outón[a,d], E. Blanco[a,d], R. García[a,b], and F. M. Morales[a,b]

[a] *IMEYMAT: Institute of Research on Electron Microscopy and Materials of the University of Cádiz, Spain.*

[b] *Department of Materials Science and Metallurgic Engineering, and Inorganic Chemistry, Faculty of Sciences, University of Cádiz, Spain.*

[c] *Institut FEMTO-ST, UMR 6174 CNRS, Université Bourgogne Franche-Comté, 15B, Avenue des montboucons 25030 Besançon Cedex, France.*

[d] *Department of Condensed Matter Physics, Faculty of Sciences, University of Cádiz, 11510 Puerto Real, Cádiz, Spain.*

* Corresponding author: antonio.santos@uca.es

Abstract: Vanadium dioxide (VO_2) is considered as one of the most promising materials for the next generation of energy-efficient smart glazing since it experiments a reversible metal-to-insulator transition at near room temperature. Nevertheless, the complexity and high cost associated to the fabrication of VO_2-based nanostructures limit the transfer of this technology to the industrial scale. Aware of this opportunity, we present a simple and advantageous method for the fabrication of VO_2 coatings on glass substrates which comprises the initial sputtering of vanadium thin films at glancing angles and the subsequent very fast oxidation of such systems in open air atmosphere. Relying on the accurate control of the thermal treatment parameters, as well as the enhanced reactivity of the high surface-to-volume porous deposited

structures, thermochromic VO_2 coatings were achieved and then characterized by means of scanning electron microscopy, grazing incidence X-ray diffraction, variable temperature UV-Vis-NIR spectrophotometry, and resistivity measurements. These investigations allowed us to determine the key role that oxidation temperatures and times not only play in modulating the optical performance of the film, but also in the surprising and advantageous decrease in the transition temperature (up to 12ºC lower than the standard value for pure VO_2), which is attained without incorporating doping agents. This fact, together with the remarkable values of luminous transmittance (~50%) and solar modulation ability (5–10%) accomplished for our best samples, opens up an alternative and simpler pathway towards the large-scale manufacturing of VO_2 coatings for smart window applications, reaching, on a preliminary basis, similar or even better performances than those obtained so far for single and undoped VO_2 films.

Keywords: Vanadium dioxide, glancing angle deposition, rapid thermal annealing, thermochromism, metal-insulator transition, smart windows.

1. Introduction

The envelope of buildings and vehicles plays a pivotal role in their energy management performance. In particular, windows are regarded as the weaker point in the covering as they account for at least 30% to 50% of the total energy lost as a result of the high thermal transfer coefficients of glazing. This leads to significant heat losses during the colder seasons and undesired heat gains in warmer times[1]. Within this framework, VO_2-based thermochromic coatings have been considered as one of the most promising routes to make construction and transportation sectors more energy-efficient. With the ability to modulate the transmission of solar energy thanks to their thermally induced reversible metal-to-insulator transition (MIT) at near room temperature (~68 ºC), which implies drastic changes in the electrical and optical properties in the near-IR range from a low temperature transparent monoclinic (M1) phase to a more heat blocking rutile (R) phase at high temperature[2,3], VO_2 systems have become one of the most widely used materials not only for smart window applications[4–8] but also for resistive switching electronics[9,10] or sensing[11,12]. For this reason, many different VO_2-based systems, fashioned as thin films, nanoparticles or 1D nanostructures, have been recently studied and developed[13–18].

For energy conservation applications, VO_2 thin films have stood out as the most suitable and straightforward alternative to directly coat glass substrates mounted in buildings[19]. In this light, many different approaches, such as sol-gel[20], physical and chemical vapor depositions[21,22], polymer-assisted deposition[23] or pulsed laser deposition[24], have been implemented to achieve VO_2 coatings. Nevertheless, the complexity and/or the high cost of the experimental requirements involved in all these methodologies, which in turn are closely linked to the complex chemistry of vanadium

and its large number of stable oxidation states, have undermined the integration of these procedures at a large scale. In this light, roll-to-roll methods are emerging as one of the most practical alternatives for the large-scale fabrication of VO_2-based coatings[25–27]. Alternatively, the post-deposition oxidation of metallic vanadium thin films has postulated as a simple and cheap practice for attaining VO_2 coatings. This approach is simpler than the more common fabrication routes if done in open air, but requires a precise control of the thermal annealing parameters to deal with the difficulties associated to the narrow process window for the formation of VO_2 (intermediary phase). Even though many different authors have covered the post-deposition oxidation of direct current (DC) magnetron sputtered vanadium films[28–32], several of these studies overlook the precise control of oxidation parameters like heating and cooling rates. These parameters become especially key during fast thermal treatments at atmospheric conditions, while others have the drawback of controlled O_2, H_2 or SO_2 partial pressures or special vacuum requirements at high temperatures (> 450ºC) for reaction times longer than 1 hour.

For that matter, our previous studies have shown that, relying on the precise control of the annealing parameters, VO_2(M1) thin films can be achieved through a simple and straightforward two-step procedure consisting of the fast oxidation in air atmosphere of sputtered V or VO_x films deposited at glancing angles[33]. However, neither the substrate (silicon) nor the precursor thicknesses (~700 nm) used on that occasion were adequate to really evaluate the feasibility of this methodology applied to the smart windows technology, which in turn purposes on finding an appropriate balance between the transition temperature (T_c) and the optical performance, defined by the luminous transmittance (T_{lum}) and the solar modulation ability (ΔT_{sol})[34]. In particular, the

current challenge is to achieve a thermochromic coating with T_c close to 25ºC, T_{lum} greater than 70%, and ΔT_{sol} of around 30%[5,7,8]. According to recent literature[35–37], it is difficult to achieve ΔT_{sol} values higher than 15% by manufacturing VO_2-based single layers with visible transmittances higher than 50%. Higher values of solar energy modulation ability (close to 30%) were also reported, although for the particular case of nanocomposites[5,7]. Nevertheless, the antagonistic relationship between these three parameters hinders the design and fabrication of VO_2-based smart coatings.

In an attempt to simplify and reduce the cost of the fabrication processes involved in the smart glazing technology, this work reports on an easy and novel route to attain high-performance VO_2 single layers deposited on glass substrates. Such a route comprises the initial DC magnetron sputtering of metallic vanadium (first step) and the subsequent fast oxidation in open air atmosphere (second step). With the purpose of enhancing the reactivity of as-deposited samples, as well as for promoting the selective and quasi-instantaneous formation of vanadium dioxide, high surface-to-volume vanadium layers with nominal thicknesses of 50 nm were deposited by GLancing Angle Deposition (GLAD). Thereupon, thanks to the precise control of the annealing parameters, the fast thermal treatment of the V−GLAD thin films was conducted in air atmosphere for different temperatures (T_r) and reaction times (τ). The microstructural, optical and electrical characterization of the oxidized systems was carried out by combing scanning electron microscopy (SEM), grazing incidence X-ray diffraction (GIXRD), variable temperature UV-Vis-NIR spectrophotometry, and resistivity measurements, allowing us to uncover the key role that reaction temperatures and times play on the development of VO_2-based thermochromic coatings of diverse nature, morphology, and unique optical and electrical features. Furthermore, an exhaustive optical study for all thermally-treated

samples is presented, placing special emphasis on the parameters of interest for specific application in smart windows (T_c, T_{lum}, ΔT_{sol}).

2. Materials and Methods

2.1. Deposition process

Films were deposited at room temperature by DC magnetron sputtering from a vanadium metallic target (51 mm diameter and 99.9 atomic % purity) in a homemade deposition chamber. Before each run, it was evacuated down to 10^{-5} Pa by means of a turbomolecular pump backed by a primary pump. The target was sputtered with a constant current density J = 100 A m^{-2}. Glass substrates (Menzel Gläser ® microscope slides) were placed at 65 mm from the target center. Porous V films with large surface-to-volume ratios and enhanced sensitivity to oxidation were deposited by GLAD. The following optimized conditions were used according to previous studies[33,38]. The incidence angle (α) of the incoming particle flux relative to the substrate normal was set at α = 85º with no rotation of the substrate (i.e., ϕ = 0 rev h^{-1}). Argon was injected at a mass flow rate of 2.40 sccm and the pumping speed was maintained at S = 13.5 L s^{-1} leading to a sputtering pressure of 0.3 Pa. The thickness of the vanadium films was measured by profilometry (Bruker DEKTAK XT 2D contact profilometer), adjusting the deposition time in order to get a nominal thickness of about 50 nm (average deposition rate of 240 nm h^{-1} for α = 85º).

2.2. Thermal treatments

After deposition, vanadium samples were thermally treated in a homemade reaction system consisting in an Al_2O_3 tube on a SiC resistors furnace being able to reach

1500°C, with an attached concentric steel tube where a high-temperature steel covered K-type thermocouple inside which acts as an axle for a system of horizontal translation. At the end of the metallic tube nearby the furnace, the thermocouple crosses and fixes to a cylinder placed inside this tube, mechanized with a hitch to hang a combustion boat. Thus, the thermometer tip is always placed some millimeters over the center of this alumina crucible, allowing the temperature in the reaction zone to be life-tracked. The other end side also crosses and is fixed to another piece that is part of a handlebar used to slide the specimen holders inside and outside (for a more detailed overview of the reaction system, refer to previous studies[13]). In this way, by fixing a temperature in the center of the furnace, one is able to control the temperature increase (heating rate) by moving the boat more and more inside the furnace. Consequently, translation routines were prepared for reaching an average heating rate of 42ºC s^{-1}, as well as for adjusting longer or shorter reaction times at a desired temperature. Lastly, all the samples were cooled down in open-air atmosphere. It should be noted here that the choice of these thermal treatment conditions is based on a preliminary study focused on the oxidation of V−GLAD thin films deposited on silicon substrates[33].

2.3. Characterizations

Plan-view scanning electron microscopy (SEM) images were acquired using FEI Nova NanoSEM operating at 5 kV in order to examine the general morphology of the films before and after each thermal treatment. GIXRD scans were performed on a Malvern PANalytical Aeris diffractometer (Cu radiation) working at 30 kV (10 mA) and setting a grazing incidence angle of 0.8°. The thermochromic optical behavior of the prepared VO_2 coatings was determined via transmission spectroscopy using an Agilent Cary 5000 spectrophotometer equipped with a custom-made temperature controlled stage.

Thus, UV-Vis-NIR transmission spectra of 250–2500 nm were recorded at selected temperatures in the range of 25–90ºC. Additionally, for the dynamic monitoring of the thermally induced phase transition, the thermal evolution of the optical transmittance at a selected NIR wavelength (2000 nm) was observed in both heating and cooling cycles at a controlled rate of 5ºC min^{-1}. DC electrical resistivity vs. temperature measurements of the oxidized films were performed in a custom-made chamber, which is covered in order to have a dark environment, using the four-probe van der Pauw geometry in the temperature range of 25–90ºC with a ramp of 1°C min^{-1} then back to 25°C with the same negative ramp. Humidity and cleanness were considered as constant. The error associated to all resistivity measurements was always below 1% and the quality of the contacts was checked prior to every run (I/V correlation close to 1) to ensure that an ohmic contact was attained on each tip (use of gold coated tips).

3. Results and discussion

3.1. As-deposited samples and subsequent thermal treatments

Keeping in mind the VO_2 layer thicknesses previously reported in the literature for smart window applications[5,6,39], 50 nm thick pure vanadium GLAD thin films were deposited on glass substrates at $\alpha = 85°$ for the additional purpose of improving their reactivity and selectivity during the following oxidation processes. **Figure 1** shows a characteristic planar view SEM micrograph of deposited samples. These observations reveal morphologies that, although being certainly porous, differ significantly from that observed for bigger thicknesses of vanadium deposited at oblique angles[33,38]. This is due to the great dependence of porosity on layer thickness for GLAD films[40], which is closely linked to the existence of two deposition regimes: a first one, dominated by

diffusive phenomena between the nuclei of material generated during the first deposition stages (limited porosity); and a second one dominated by shadowing events that take place after exceeding a certain threshold thickness (increasing porosity with thickness)[41,42]. In addition to the foregoing, profilometry measurements carried out on different regions within a same specimen determined a real layer thicknesses of 70 ± 5 nm, which is superior than expected. This fact finds an explanation in the rising of porosity (deposition processes dominated by the shadowing effect), which shows that the deposited V-GLAD films are porous enough to fulfill the purposes that will be addressed in this study (for more information on the evolution of porosity as a function of GLAD layer thickness, refer to Supplementary Material Section I).

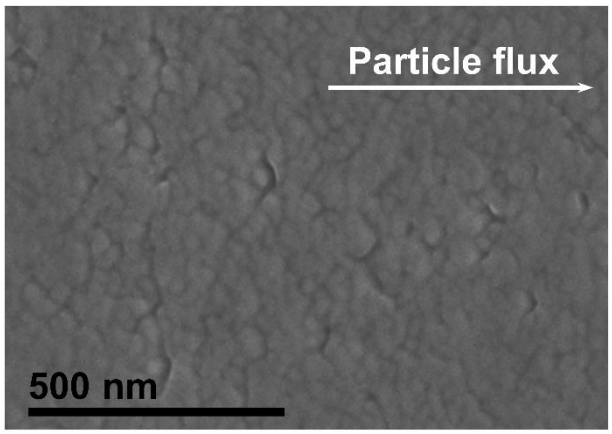

Figure 1. Planar view SEM micrograph of an as-deposited vanadium GLAD film. The white arrow indicates the direction of the particle flux during GLAD deposition.

Afterwards, samples were undergone to different rapid thermal treatments to promote the formation of the VO_2 thermochromic phase. For all cases, the heating rate was fixed at 42 ºC s^{-1}, whereas reaction temperatures (T_r) and times (τ) were varied between 475–575ºC and 1–35 seconds, respectively, with the aim of optimizing the oxidation

conditions. Finally, all samples were cooled down to room temperature in air atmosphere. A detailed scheme of the fast thermal treatment procedure can be found in **Figure 2**. It is worth mentioning that all the displayed temperature vs. time tracks are the ones recorded during the thermal treatment, which emphasizes the high control achieved over the thermal treatment parameters. Likewise**,** all treated samples, together with their treatment conditions and nomenclature, are listed in **Table 1**.

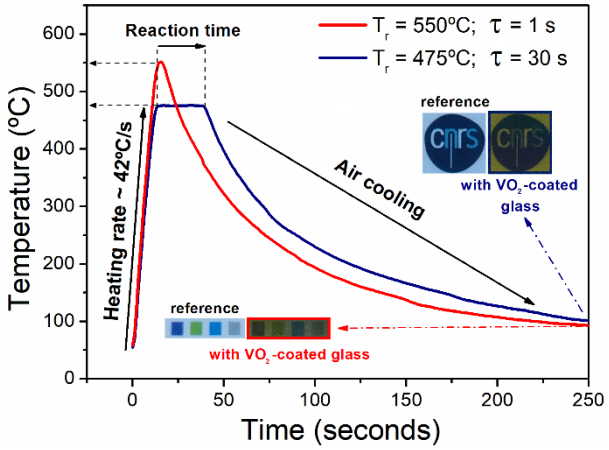

Figure 2. Example of the temperature vs. time tracks registered for two thermally treated samples. The different captions and insets place emphasis on the different stages involved during the thermal treatment as well as the sample aspect once oxidized.

Table 1. Thermal treatment conditions for the samples referred in this study. T_r is the reaction temperature and τ is the reaction time.

Sample	T_r (ºC)	τ (s)
475_15	475	15
475_25	475	25
475_30	475	30
475_35	475	35
500_1	500	1
525_1	525	1
525_5	525	5
550_1	550	1
550_5	550	5
550_10	550	10
575_1	575	1

3.2. Oxidized samples

Once all samples are thermally treated, their comprehensive microstructural, optical and electrical characterization will be addressed not only to know and correlate the effect that the different heat treatment parameters produce on the morphologies, oxides synthesized and performances achieved, but also to assess the practical viability of the methodologies and systems developed here in order to be integrated into smart glazing.

3.2.1. Surface and crystalline microstructure

Figure 3 displays structures and morphologies (top-view SEM micrographs) after annealing of V-GLAD samples to 475ºC and 550ºC and different reaction times. First of all, it must be highlighted the great difference between the microstructures obtained here and those achieved in previous studies for similar heat treatments and vanadium samples on silicon substrates[33] (VO_2 films on silicon were characterized by larger and

more ordered grains forming mosaic-like structures). Arrangements attained in this study are much more disordered, formed by smaller and non-equiaxed grains, which are slightly elongated along the axial direction. Also note that this last fact is even observed for samples subjected to the shortest oxidation times (1 and 15 seconds). This means that structures synthesized on glass substrates have an apparently higher overall porosity than those obtained on silicon, which can translate into an important optical advantage. Therefore, although the thickness of the layer can also play an important role, it seems that the kind of microstructures obtained after oxidation, and thus the conditions of the thermal treatment to reach a certain VO_2 yield, depends on some extent on the nature of the substrate as well as its ability to conduct/dissipate heat. On another note, these SEM observations make us think that all samples, including those thermally treated for a few seconds, have been fully oxidized, which can be linked to the improved reactivity of GLAD thin films. This assumption is also supported by the photographs included in **Fig. 2**, which show the relatively transparent appearance of the samples once oxidized. Nonetheless, the thermal treatment induces a loss of the porous structure so characteristic of these systems (ordered and slanted nanocolumns), which improves the overall transmittance of the coating, allowing the tuning of its effective refractive index and acting as an anti-reflective layer.

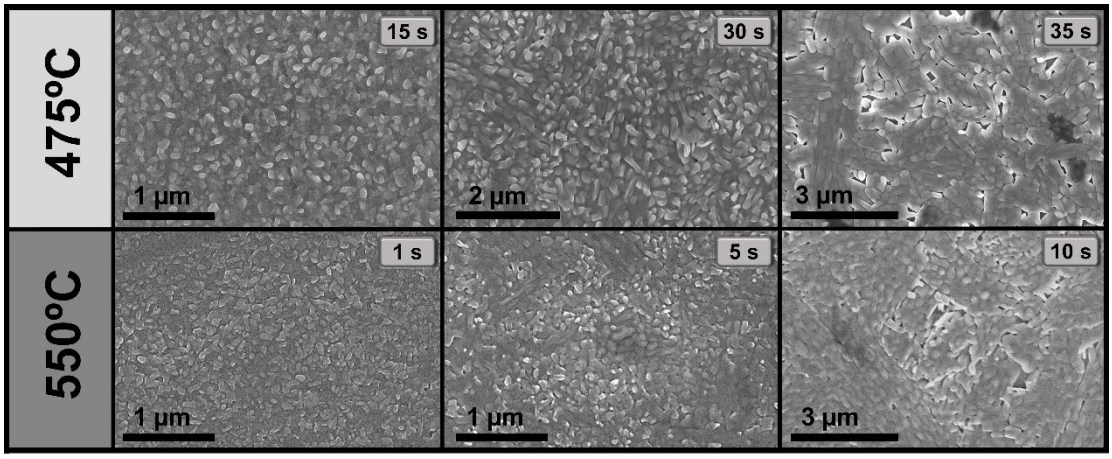

Figure 3. SEM planar views of samples subjected to rapid thermal treatments at T_r = 475ºC and 550ºC, and reaction times (τ) ranging from 1 to 35 s as labelled in the images.

Concerning the effect of reaction temperatures and times on the size and shape of the generated microstructures, it can be observed that the simultaneous increase of both parameters leads to the gradual formation of bigger and randomly distributed grains. Moreover, the growth along the axial direction is also favored at higher T_r and τ, although much more limited when compared to the microstructures achieved by oxidizing thicker V-GLAD samples on silicon for longer reaction times (> 60 s)[33]. In this way, to achieve a granular structure of a determined grain size, we could either increase the temperature or the reaction time. This makes the microstructures of samples 475_15 and 550_5 a priori comparable. The same applies for samples 475_35 and 550_10. However, the choice of one or the other approach could have a significant effect not only on the synthesis of different vanadium oxides or polymorphs, but also on the optical performance of the coating, even if they present similar microstructures. Similarly, this fact could also promote the preferential diffusion of matter towards

specific areas to the detriment of others, so that, starting from the same volume of vanadium, different sample thicknesses and, therefore, microstructures could be found.

In order to corroborate the above assumptions, GIXRD studies were carried out on several samples before and after the thermal treatments. As can be seen in **Figure 4**, the as-deposited sample is crystallized (note the diffraction peak (111) corresponding to vanadium metal). It is also observed how all oxidized samples, apart from being polycrystalline, contain, to a greater or lesser extent, VO_2(M) (JCPDS Card No. 03-65-2358), which is accompanied with the disappearance of the diffraction peak corresponding to metallic vanadium. This, in addition to being in agreement with the abovementioned, would confirm the full oxidation of the deposited V-GLAD films even for those samples subjected to instantaneous thermal treatments (see diffractograms recorded for samples 525_1 and 550_1). Similarly, the formation of oxides with a stoichiometric ratio lower (V_2O_3, JCPDS Card No. 00-085-1411; sample 475_15) and higher (V_2O_5, JCPDS Card No. 00-041-1426; samples 475_30 and 550_5) than that of the dioxide was also evidenced for moderate and high T_r and τ combinations, respectively, which could play a pivotal role in the optical response of the coating. In contrast, it seems that instantaneous treatments favor the exclusive synthesis of VO_2. Additionally, it is also noteworthy how samples 475_15 and 550_5, both with a similar surface microstructure, exhibit different compositions and crystallinities. Therefore, this fact leads us to conclude that such samples are not directly comparable from the point of view of their optical responses.

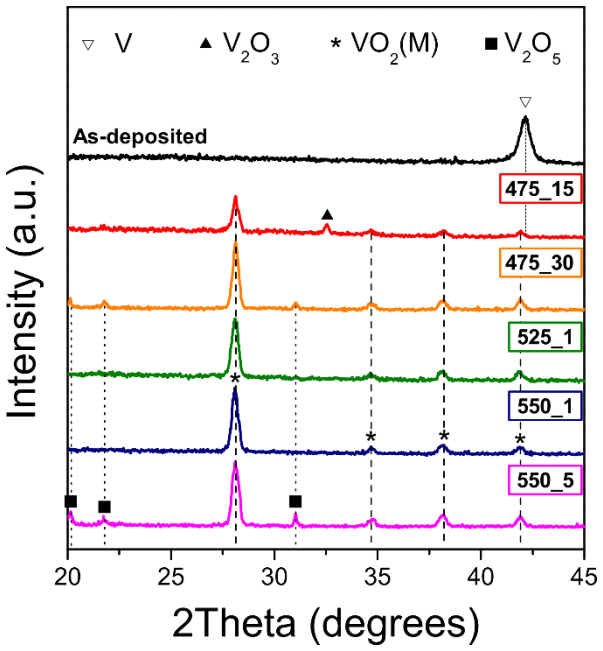

Figure 4. GIXRD diffractograms for an as-deposited vanadium GLAD film as well as for different samples subjected to rapid thermal treatments at T_r = 475ºC, 525ºC and 550ºC, and reaction times (τ) ranging from 1 to 30 s as labelled in the images.

3.2.2. Optical characterization

Once the microstructures resulting from the different rapid heat treatments have been examined, their optical performances have to be evaluated for application in smart windows, which will also give us a qualitative idea of the VO_2 yields achieved. To meet this goal, vis-NIR transmittance spectra were collected for all oxidized samples at 25ºC and 90ºC (**Figure 5**), which were arranged attending to their T_r (475ºC and 550ºC) or τ (1 s). Additionally, in order to facilitate the understanding while quantitatively assessing the thermochromic features of such fabricated coatings, **Table 2** collects the values of the different optical performance parameters calculated as described by Outón et al.[20].

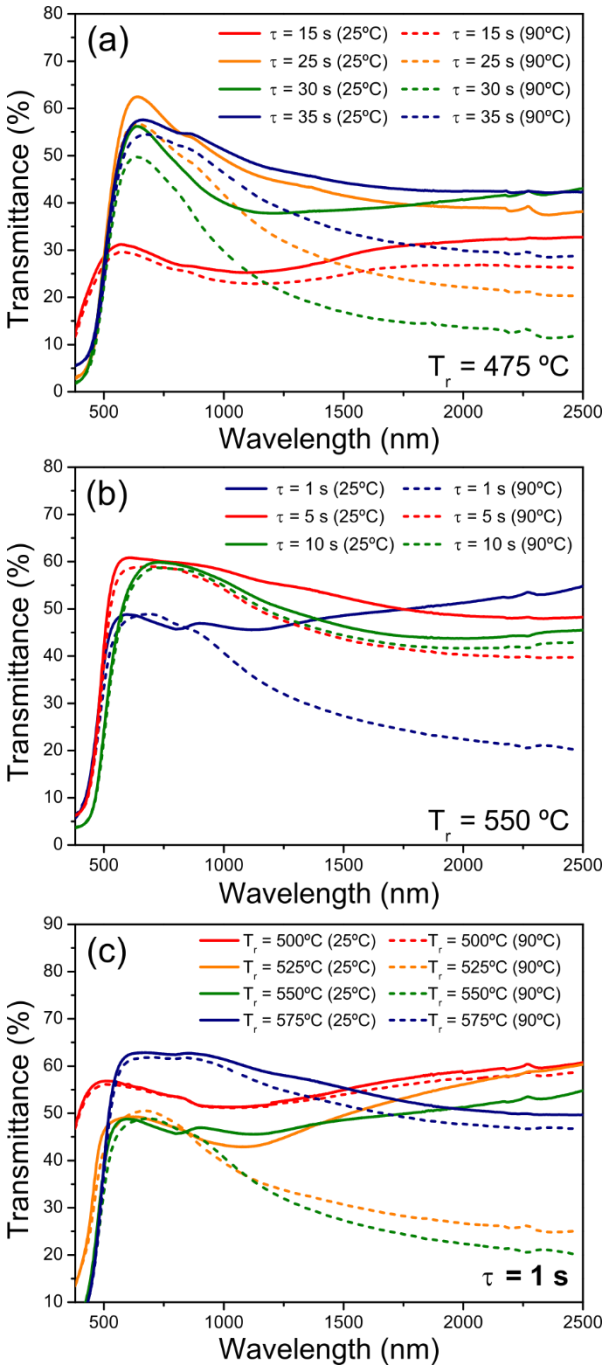

Figure 5. Transmittance spectra recorded at 25ºC (solid lines) and 90ºC (dashed lines) for samples thermally treated: at (a) 475ºC and (b) 550ºC for τ ranging from 1 to 35 s; (c) during 1 s for T_r ranging from 500ºC to 575ºC.

In the first instance, we will focus on the results obtained for samples treated at 475ºC (**Fig. 5(a)**). Based on the absolute transmittance drops with temperature, it can be preliminarily assumed that VO_2 synthesis at 475ºC is maximized for reaction times between 25–30 s. In the near-infrared region, drops are less pronounced for longer (35 s) and shorter (15 s) reaction times. The signature exhibited by such transmittance spectra is also a matter of interest. In this sense, it should be noted that the spectra displayed in **Fig. 5(a)** differ considerably from the one previously reported for a 50-nm-thick coating of pure VO_2(M1)[43]. By contrast, they are very similar to those registered for pure[44], doped[45–47] and aged[48] VO_2 films. However, most authors claim the manufacture of pure VO_2 layers on the grounds of the existence of a certain thermochromic behavior and do not consider the possible synthesis of other unwanted vanadium oxides. The latter, in addition to being the most likely scenario given the difficulties associated with the synthesis of VO_2 mentioned above, could also explain the optical response of the materials fabricated in this work. Thereby, it could be stated that all samples treated at 475ºC are composed, to a greater or lesser extent, by vanadium dioxide (since all of them exhibit a drop of transmission when increasing temperature) accompanied by other vanadium oxides. This is in fine agreement with what was previously observed by GIXRD (**Fig. 4**). Furthermore, taking as reference several studies reporting the optical properties of V_2O_5[49] and V_2O_3[50] thin films, while considering the trends observed in the V-O phase diagram[51,52], it could be suggested that sample 475_15 would be composed by VO_2 and VO_{2-x} mixtures, mainly V_2O_3, with $0 < x < 2$, which are characterized by moderate solar modulation abilities and greater transmittances in the NIR than in the visible range. On the other hand, samples 475_25/30/35 would be formed by VO_2 and VO_{2+x} mixtures, mainly V_2O_5,

with x > 0, presenting higher transmittance values in the visible than in the NIR range and/or maximum peaks of transmittance at ~600 nm (V_2O_5 fingerprint).

Table 2. Radiometric and photometric parameters change with heating for all studied samples. For a detailed definition and explanation of how all these parameters are obtained, refer to the work of Outón et al. (Appendix A)[20].

Sample	T_{lum} (%)	ΔT_{lum} (%)	ΔT_{sol} (%)	$\Delta T_{sol, rel}$ (%)	ΔT_{IR} (%)	$\Delta T_{IR, rel}$ (%)
475_15	29.5	1.6	2.0	7.3	2.6	9.6
475_25	47.2	4.3	6.2	14.3	9.8	20.5
475_30	41.9	4.8	8.4	21.7	13.9	33.6
475_35	43.7	3.1	4.2	9.6	6.6	13.3
500_1	56.1	0.6	0.5	0.9	0.5	0.9
525_1	47.4	1.2	4.2	9.6	9.1	19.4
525_5	49.6	4.0	5.4	12.5	9.3	19.8
550_1	44.6	2.5	5.1	12.2	10.5	22.3
550_5	54.2	3.0	3.3	7.2	5.2	10.2
550_10	42.7	1.5	1.2	2.6	1.4	2.6
575_1	54.6	1.8	1.6	3.0	2.2	3.7

Afterwards, the optical performance of samples annealed at 475ºC is evaluated by means of their radiometric (T_{sol}) and photometric (T_{lum}) values. As listed in **Table 2**, the VO_2 + VO_{2+x} mixtures provide the best optical responses, with samples 475_25 and 475_30 reaching the maximum values of T_{lum} (47.2%) and ΔT_{sol} (8.4 %), respectively. In this connection, the great values of ΔT_{sol} achieved for samples 475_25 and 475_30 can only be explained by the significant variations of transmittance that they show in the visible wavelengths at 25ºC and 90ºC (ΔT_{lum} > 4%), range in which solar radiation peaks. This phenomenon has also been observed in several previous works[44,53,54], although none of them tried to identify its cause. In general, it can be seen that all of

them have something in common: the presence of sharp transmittance peaks at ~600 nm at room temperature, which suggests that this beneficial event can be related to the coexistence of the VO_2 and V_2O_5 phases. Last but not least, it must be also emphasized the valuable information that the relative values of solar modulation in the near infrared ($\Delta T_{IR,\,rel}$) can provide us, since, unlike the ΔT_{sol} values, these are not affected by T_{lum} variations. So they can be considered as significant indicators/comparators of the VO_2 yields achieved (take care not to confuse this information with the real percentage of VO_2 of a sample). In this way, the amount of VO_2 generated at 475ºC can be monitored, which initially increases with time until reaching a maximum for a reaction time of 30 s (**Table 2**).

When the annealing temperature is 550ºC (**Fig. 5(b)**), a narrowing of the reaction time window for the synthesis of vanadium dioxide is observed. Based on the criteria developed for samples treated at 475ºC, it could be said that sample 550_1 presents the greatest interest for application in smart windows. It combines an abrupt drop in transmittance in the NIR range with a high transmittance in the visible range. Besides, the spectra recorded for this sample at 25ºC and 90ºC are quite similar to those obtained for thin layers of pure vanadium dioxide, highlighting the high VO_2 content of this sample[43]. On another note, longer oxidation times only lead to the formation of VO_{2+x} mixtures together with decreasing amounts of VO_2 as the oxidation time increases. Nonetheless, it must be highlighted the noticeable value of T_{lum} (54.2%) achieved for sample 550_5 (**Table 2**), which may be partially promoted by the changes in the microstructure of the coatings (increase of the overall porosity) as τ and T_r increase (see **Fig. 3**). Note that, according to previous works[23,55,56], the introduction of porosity can improve the anti-reflective properties of VO_2 coatings by modulating the optical

constants (*n*, *k*), leading to T_{lum} values above 40%. This fact, as well as the acceptable value of ΔT_{sol} (3.3%) attained for this sample despite its fairly narrow absolute drop in transmittance with temperature when comparted to that observed in sample 550_1 (ΔT_{sol} = 5.1%), can be associated, according to GIXRD studies, with the presence of V_2O_5, which is also manifested through a remarkable decrease in transmittance at 90ºC within the 380–1000 nm wavelength range. Moreover, it can also be seen that such amounts of V_2O_5 increase progressively for longer reaction times (note that the spectra obtained for the sample 550_10 are quite similar to those obtained for pure V_2O_5 films[49]). All the above is in good agreement with the values of $\Delta T_{IR,\,rel}$ calculated for samples annealed at 550ºC, which reveal the progressive decrease of VO_2 yields experienced for τ between 1 and 10 seconds.

Fig. 5(c) collects the spectra resulting from the fast thermal treatment of V-GLAD samples undergone to 1-second reaction time when varying the oxidation temperature from 500ºC to 575ºC. As can be noted, the reaction temperature window for the flash annealing of VO_2 is limited to 525–550ºC, with samples 500_1 and 575_1 presenting what appears to be mixtures of VO_{2-x} and VO_{2+x}, respectively, along with small quantities of VO_2. Besides, the spectral signatures of samples 525_1 and 550_1 again suggest that they are mainly composed by VO_2 accompanied by slight fractions of VO_{2-x} and/or VO_{2+x} mixtures. This is also supported by the fact that these two samples have quite similar optical behaviors (for more information, refer to **Table 2**). Therefore, it is shown that the refinement in VO_2 of these thermochromic coatings can only be achieved by reducing the reaction time of the heat treatment to a minimum of 1 s when operating within the temperature range of 525–550ºC.

In view of all the above, it becomes clear that there are two possible pathways to attain VO_2-based thermochromic coatings with potential application for smart windows by means of the fast and finely controlled thermal treatment of 50 nm thick V-GLAD samples: (i) at 475ºC and τ = 25–30 s; or (ii) for 1 s with T_r ranging from 525ºC to 550ºC. As a link between these two routes, it is also noteworthy the particular case of sample 525_5 (to see the transmittance spectra of this sample at 25ºC and 90ºC, refer to Supplementary Material Section II), whose optical behaviors are quite similar to that of sample 475ºC_25. This fact opens an alternative route to meet optical performances similar to those attained at 475ºC, although with much less control over reaction times. Likewise, as expected from results in previous sections, samples with comparable microstructures in terms of morphology and grain sizes (i.e., the pairs 475_15 / 550_5 and 475_35 / 550_10) presented very different optical behaviors, which hinders the establishment and understanding of the structure-properties relationships in these materials.

Thereupon, the features of the MIT for the best samples were examined from the kinetic evolution of transmittance at 2000 nm on heating and cooling at a constant rate (**Figure 6** and **Figure 7**). Furthermore, **Table 3** lists the transition temperatures, for heating ($T_{c(H)}$) and cooling ($T_{c(C)}$), which are calculated from the derivative curves of the transmittance plots (**Fig. 6(a)** and **Fig. 7(a)**) with a Gaussian fit (see **Fig. 6(b–c)** and **Fig. 7(b–d)**), along with the hysteresis loop width (W_H), transmittance at 2000 nm for 25ºC (T_{max}) and for 90ºC (T_{min}), and their relative difference.

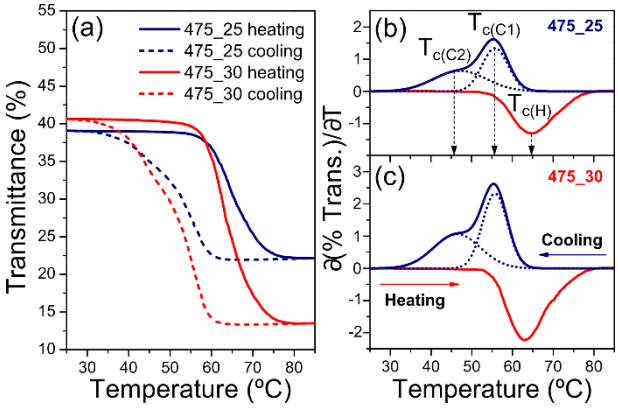

Figure 6. (a) Thermal evolution of the optical transmittance at 2000 nm of 475_25 (blue) and 475_30 (red) samples for heating (solid lines) and cooling (dashed lines). Derivative of each kinetic thermochromic cycle for samples (b) 475_25 and (c) 475_30 for heating (red) and cooling (blue). For a better overview, the derivatives of the cooling are plotted in absolute values.

On the one hand, the studies related to the evolution of transmittance with temperature at 2000 nm for samples 475_25 and 475_30 (**Fig. 6**) reveal asymmetric hysteresis loops in both cases, which stem from the development of two different slopes (the first steeper; the second more gradual) when cooling through the MIT. This leads to two different transition temperatures on cooling cycles ($T_{c(C1)}$ and $T_{c(C2)}$), associated with high and low $T_{c(C)}$, respectively. Besides, both samples exhibit very similar values of $T_{c(C1)}$ and $T_{c(C2)}$, with minimum variation rates (absolute minimum of the derivatives of the optical hysteresis during cooling cycles) at $T_{c(C1)}$ = 56ºC. Conversely, this phenomenon does not occur during the heating cycles, giving rise to single transition temperatures that are slightly lower ($T_{c(H)}$ = 65ºC and 63ºC for samples 475_25 and 475_30, respectively) than those reported for pure VO_2 films (~ 68ºC). This results in variable hysteresis widths of 9–18ºC and 7–17ºC for 475_25 and 475_30, respectively.

Table 3. Main features of the thermochromic hysteresis loops illustrated in **Fig. 6** and **Fig. 7**: $T_{c(H)}$ denotes the temperatures of the MIT transition on heating; $T_{c(C1)}$ and $T_{c(C2)}$ indicate the temperatures of the MIT on cooling. W_{H1} and W_{H2} are the hysteresis loop widths given by $T_{c(H)} - T_{c(C1)}$ and $T_{c(H)} - T_{c(C2)}$, respectively. T_{max}, and T_{min} denote the 2000 nm wavelength transmittances at 25ºC and 90 ºC. ΔT_{rel} is the relative decrease of transmittance upon the transition at 2000 nm.

Sample	**$T_{c(H)}$ (ºC) heating**	**$T_{c(C)}$ (ºC) cooling**		**W_H (ºC)**		**T_{max} (%)**	**T_{min} (%)**	**ΔT_{rel} (%)**
		C1	**C2**	**1**	**2**			
475_25	65	56*	47	9	18	39.1	22.1	43.5
475_30	63	56*	46	7	17	40.6	13.5	66.7
525_1	61	49	–	12	–	56.0	26.6	52.5
525_5	65	57*	42	8	23	45.0	22.7	49.6
550_1	56	43	–	13	–	51.2	22.4	56.2

* Main peak

According to the literature, two-step metal-to-insulator transitions during cooling would originate from the physical structure of the VO_2[57], and more specifically from the presence of crystal grains with different sizes[19]. This is in agreement with the SEM micrographs of these two samples (see **Fig. 3**). Additionally, this event could correlate with the emergence of V_2O_5, which would be responsible for the gradual growth of some of these grains along the axial direction[33]. By contrast, the decrease in T_c for non-doped VO_2 coatings has been linked to such disparate causes as oxygen-deficiency-related defects[58,59], the presence of residual stress near the VO_2 film-substrate interface[60–62], or the internal compressive stress due to mismatch shrinkage between VO_2(M) and V_2O_5 during the cooling stage[63]. Indeed, this last theory would even reinforce our previous assumption which relates the appearance of asymmetric

hysteresis loops during the cooling stage to the presence of V_2O_5. Nonetheless, although so far no consensus has been reached on the origin and mechanism associated with this phenomenon, any of the above casuistry could partially account for the lowering of the transition temperature for the systems addressed in this study. In turn, this phenomenon would also imply a clear advantage over elemental VO_2 doping, which has been shown to have a negative effect on optical performance[64].

Ultimately, the comparison of the ΔT_{rel} values obtained for the two best thermally treated samples at 475ºC once again reveal the higher VO_2 content of the 475_30 sample. This fact, together with the good balance achieved for the parameters that determine the applicability of VO_2-based coatings in smart windows (i.e., T_c, T_{lum} and ΔT_{sol}), makes 475_30 the most interesting sample within the series of heat treatments carried out at 475ºC. In order to have a better insight into the joint evolution of these three key parameters during the heating-cooling cycle, **Figure 8(a)** displays the Vis-NIR transmission spectra of sample 475_30 registered at gradually increasing or decreasing temperatures. The noticeable difference between the set of spectra recorded for the heating and cooling stages (note they were recorded for equivalent temperature intervals centered on the T_c values) again highlights the asymmetric hysteresis characteristic of this sample.

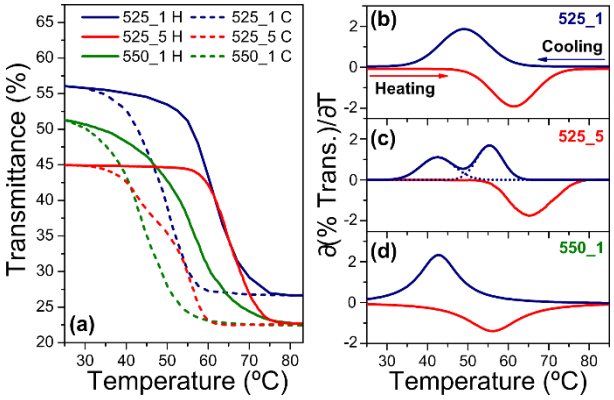

Figure 7. (a) Thermal evolution of the optical transmittance at 2000 nm of 525_1 (blue), 525_5 (red) and 550_1 (green) samples for heating (solid lines) and cooling (dashed lines). Derivative of each kinetic thermochromic cycle for samples (b) 525_1, (c) 525_5 and (d) 550_1 on heating (red) and cooling (blue). For a better overview, the derivatives of the cooling are plotted in absolute values.

On the other hand, **Fig. 7** shows the different thermal evolutions of transmittance experienced by the samples subjected to shorter oxidation times at 525ºC and 550ºC. Once again, it can be appreciated that the optical behavior of sample 525_5 (**Fig. 7(a)** and **Fig. 7(c)**) is quite similar to that observed for 475_25, presenting asymmetric hysteresis loops although wider variable W_H values of 8–23ºC as a consequence of the emerging of two slopes more clearly differentiated during the cooling cycles. However, samples annealed at τ = 1 s exhibit rather different optical performances from those seen so far in this study. The first distinguishing feature is the arising of single slopes during each heating-cooling cycle (see **Fig. 7(b)** and **Fig. 7(d)**). The second one is the outstanding decrease in T_c values for heating, which becomes minimum for sample 550_1 ($T_{c(H)}$ = 56ºC). Therefore, it seems that this phenomenon, which was previously related, among other causes, to oxygen vacancies, is accentuated by reducing the

oxidation time to a minimum of 1 s, so that the oxidation would occur so rapidly that stoichiometry O/V = 2 is not completely reached. For the rest, samples 525_1 and 550_1 show comparable W_H, T_{max} and T_{min} values at 2000 nm, with the former displaying a quasi-symmetrical hysteresis loop (see **Fig. 7 (a–b)**). This symmetry is also highlighted in **Fig. 8(b)**, which displays the transmission spectra of sample 525_1 collected at multiple temperatures during heating-cooling cycles. This leads us once again to conclude that the appearance of asymmetric hysteresis loops during cooling is an inherent characteristic of the presence of V_2O_5.

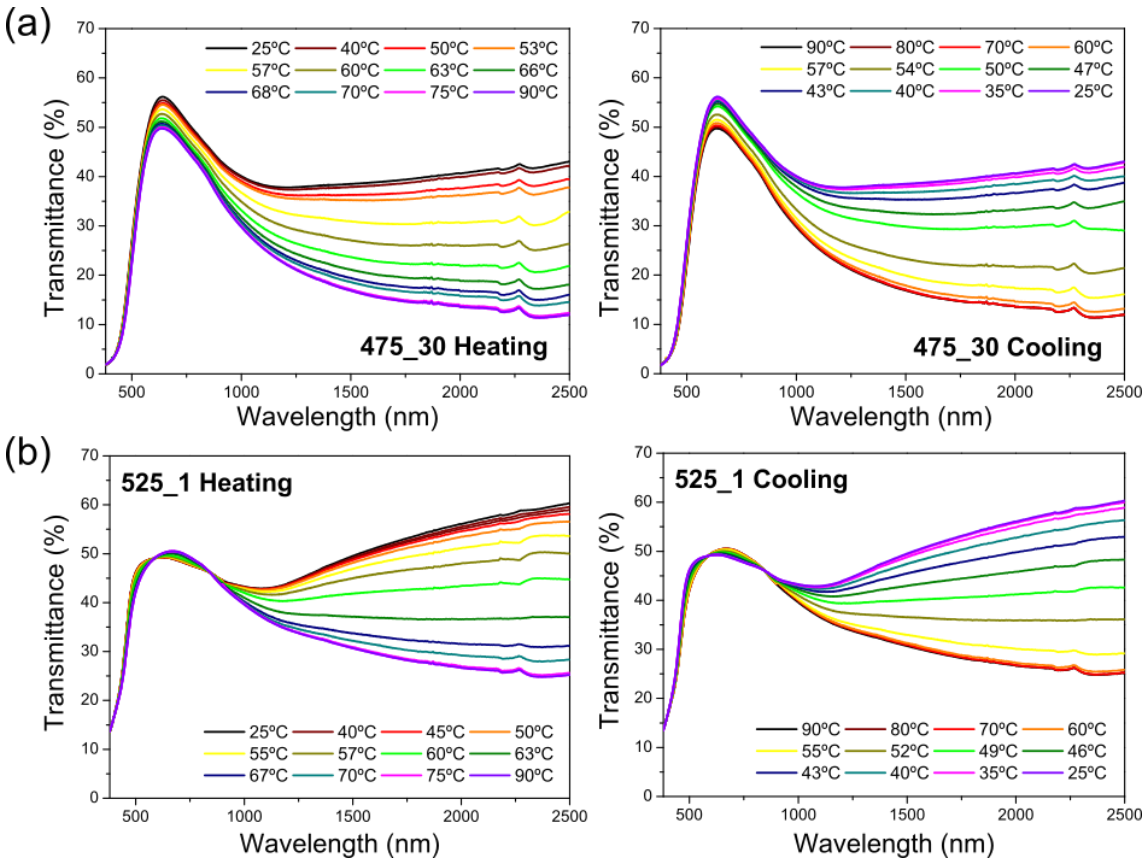

Figure 8. Vis-NIR transmission spectra of samples (a) 475_30 and (b) 525_1 recorded at gradually increasing (left) or decreasing (right) temperatures.

Next, the analysis of all results obtained until this point will be addressed from an overall perspective. In general, it can be seen how the increase in VO_2 yields, which has a direct impact on the increase in ΔT_{sol} values, results in noticeable decreases in T_{lum} values. In the same way, it is observed that T_c values, in addition to decreasing together with T_{lum} (or what is the same, when ΔT_{sol} increases), exhibit a gradual drop as the reaction temperature increases for the same reaction time (τ = 1 s). Also note that this effect becomes slightly accentuated as VO_2 contents enhances (to see the particular case of samples 475_25 and 475_30 with $\Delta T_{IR,\,rel}$ values of 13.3% and 33.6%, respectively). All this further supports the hypothesis that the shift of the MIT towards lower temperatures would be mainly due to oxygen deficiency in VO_2.

Similarly, it is also interesting to assess the results obtained for each of the two optimal performance pathways. In this regard, although the best samples all have T_{lum} values in-between 40–50%, samples thermally-treated for 25–30 seconds at 475°C are characterized by higher ΔT_{sol} values (6.2–8.4%) which are due to significant drops in visible transmittance when increasing the temperature. On the contrary, samples undergone to instantaneous annealing (τ = 1 s) within the temperature range of 525–550ºC show remarkable T_c drops of 7–12ºC bellow the values reported for pure VO_2 structures, which would not find its origin in the elemental doping but rather to the oxygen-deficiency-related defects promoted when limiting oxygen consumption times.

Once come to this point, it is necessary to highlight the importance of the results obtained in the present work: although the luminous transmittances reached here are not high enough, which is rather an inherent characteristic of VO_2(M1), remarkable

balances between the parameters T_{lum} and ΔT_{sol} are achieved, equaling or even improving (decrease of T_c without doping) the best results achieved so far for non-doped single VO_2 coatings[5,39,65], as well as those attained in our previous studies on the atmospheric flash oxidation of dense vanadium nanolayers[66]. Furthermore, it is worthwhile to mention the not excessively high visible transmittance of the glass substrate employed in these studies (~82% of average transmittance in-between 380–750 nm). Since this leads to a limitation in optical performance, values of T_{lum} and ΔT_{sol} were recalculated after disregarding the negative effects coming from the glass substrate, so only the contribution of VO_2-based layers was explored (see Supplementary Material Section III). These new calculations resulted in a considerable improvement of the two thermochromic performance parameters, leading to an increase of T_{lum} and ΔT_{sol} values of ~22% and ~16%, respectively. This makes these two parameters reach values of 51.0% and 9.8%, respectively, for the sample 475_30; or 54.2% and 5.8%, respectively, for the 550_1.

3.2.3. Electrical characterization

Finally, for the further purpose of exploring the electronic features of the systems developed here, **Figure 9** displays the resistivity vs. temperature measurements. They were conducted on the samples that showed the highest solar modulation abilities (i.e. samples 475_25 and 475_30 according to **Table 2**). In this regard, it should be noted that these measurements were also carried out for other samples such as 525_1 or 550_1, but their moderate ΔT_{sol} values, together with the additional challenge of studying very thin layers (< 100 nm), did not allow us to register conclusive outcomes for all of them. As can be seen in **Fig. 9**, the asymmetric hysteresis previously observed

for both 475_25/30 samples through their optical characterization on heating becomes less evident in electrical resistivity measurements, which is a consequence of the flattening of the multiple slopes when plotting the logarithm of the resistivity[57].

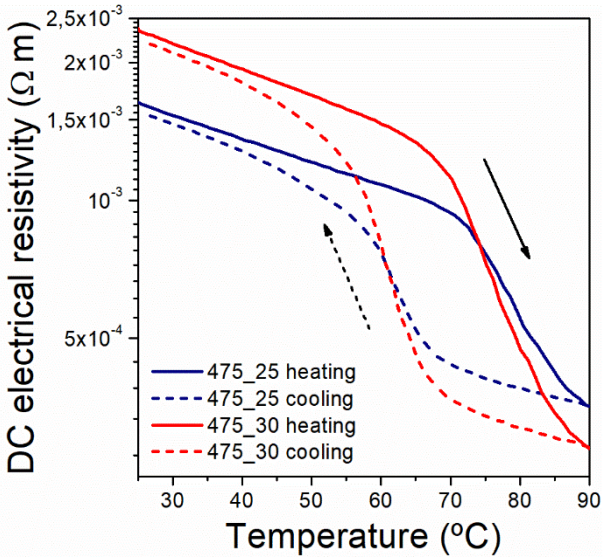

Figure 9. Changes in electrical resistivity with temperature registered for the samples 475_25 (blue) and 475_30 (red) during heating (solid lines) and cooling cycles.

Notwithstanding, the analysis of the derivative resistivity curves only enables the determination of single transition slopes during both heating and cooling cycles, which, in contrast to what was observed through the optical characterization of these same samples, leads to single values of T_c and W_H (see Supplementary Material Section IV), these latter being comparable to the central values of the hysteresis width intervals defined in the previous section. Also noteworthy is the significant increases in T_c recorded during the heating ($T_{c(H)}$ = 77ºC and 73ºC for 475_25 and 475_30, respectively). This discrepancy between the transition temperatures extracted from

optical and electrical measurements was also observed in previous studies[67], which is explained by the fact that the structural phase transition (SPT) of VO_2 does not directly induce the MIT (although the SPT and the MIT are likely correlated to each other). On the other side, it can be appreciated that heating and cooling cycles induce electrical resistivity changes that never exceed an order of magnitude, which are affected by both layer thicknesses (the thicker, the sharper the plunge in resistivity) and VO_2 yields. Hence, at equal thickness, the larger resistivity drops registered for sample 475_30 (~0.9 orders of magnitude) compared to 475_25 (~0.7 orders of magnitude) again reveal its higher VO_2 content.

All in all, it can be determined that, in general, the outcomes obtained from the electrical characterization of these samples lead to the same general conclusions as those reached by means of optical studies, although with small nuances inherent to each technique itself.

4. Conclusions

A simple two-step approach for the effective oxidation of porous vanadium films to attain VO_2-based thermochromic coatings of unique and advantageous properties for smart glazing applications has been reported. After the observation of the outcomes obtained throughout the fast oxidation of several 50 nm thick vanadium samples sputtered on glass substrates by the GLAD method, it is concluded that the selective formation of different vanadium oxides can be achieved simply by finely controlling oxidation temperatures and times. In this context, it must be also highlighted that these thermal oxidations involve green-like reactions, only using the power for heating a tube open to the atmosphere, without the further assistance of neither reactive gases or

catalysts nor special vacuum or pressure requirements. The outcomes obtained from the microstructural and functional (optical and electrical) characterization of such oxidized samples evidenced two optimal pathways for synthesizing high-performance VO_2-based coatings with unique thermochromic features: (i) a first one at 475ºC and τ = 25–30 s, characterized by the formation of VO_2 + VO_{2+x} (x > 0) mixtures; and (ii) a second one for τ = 1 s and temperatures ranging from 525–550ºC, leading to higher VO_2 yields. In addition to the good balance reached for T_{lum}, T_{sol} and T_c parameters through both optimal synthesis routes, which is indeed key when considering smart window applications, it should be noted that samples achieved at 475ºC showed particularly high ΔT_{sol} values (6–9%), which are promoted by the significant transmittance drops that they experience at 380–1000 nm. On another note, samples oxidized at the minimum oxidation time showed T_c values (without doping) for heating up to 12ºC below the normal value reported for pure VO_2 (~68ºC), which was mainly associated with the formation of oxygen-deficiency-related defects (oxygen vacancies). For all the reasons listed above, it is thought that the methodologies described in this work can contribute significantly to the development of simpler and more profitable strategies for the large-scale manufacture of VO_2-based smart glazing, not only leading to thermochromic responses that equal or even outperform those achieved so far through more complex and/or expensive procedures, but also still leaving much room for improvement (elemental doping, thickness optimization, etc.).

Acknowledgements

A. J. Santos would like to thank the University of Cádiz and the Spanish Ministerio de Universidades for the concession of a “Margarita Salas” postdoctoral fellowship funded by the European Union - NextGenerationEU (sol-202100211960-tra). J. Outón acknowledges the support by the Spanish Ministerio de Educación y Cultura through grant FPU19-02638. University of Cádiz and IMEYMAT are also acknowledged by financing the mutual facilities available at the UCA R&D Central Services (SC-ICYT), the UCA project references “PUENTE PR2020-003” and “OTRI AT2019/032”, and the IMEYMAT project reference “LÍNEAS PRIORITARIAS PLP2021120-1”. This work was supported by the Spanish State R&D project (Retos y Generación de Conocimiento) ref. PID2020–114418RBI00. The regional government of Andalusia with FEDER co-funding also participates through the projects AT-5983 Trewa 1157178 and FEDER-UCA18-10788. This work was partly supported by the french RENATECH network, FEMTO-ST technological facility, by the Region Bourgogne-Franche-Comté and by EIPHI Graduate School (Contract “ANR–17–EURE–0002”).

Data availability statement

The raw/processed data required to reproduce these findings cannot be shared at this time due to technical or time limitations.

Declaration of Competing Interest

The authors declare that they have no known competing financial interests or personal relationships that could have appeared to influence the work reported in this paper.

REFERENCES

[1] K. Khaled, U. Berardi, Current and future coating technologies for architectural glazing applications, Energy Build. 244 (2021) 111022. doi:10.1016/j.enbuild.2021.111022.

[2] H. Lu, S. Clark, Y. Guo, J. Robertson, The metal-insulator phase change in vanadium dioxide and its applications, J. Appl. Phys. 129 (2021) 240902. doi:10.1063/5.0027674.

[3] Z. Shao, X. Cao, H. Luo, P. Jin, Recent progress in the phase-transition mechanism and modulation of vanadium dioxide materials, NPG Asia Mater. 10 (2018) 581–605. doi:10.1038/s41427-018-0061-2.

[4] S. Wang, M. Liu, L. Kong, Y. Long, X. Jiang, A. Yu, Recent progress in VO_2 smart coatings: Strategies to improve the thermochromic properties, Prog. Mater. Sci. 81 (2016) 1–54. doi:10.1016/j.pmatsci.2016.03.001.

[5] Y. Cui, Y. Ke, C. Liu, Z. Chen, N. Wang, L. Zhang, Y. Zhou, S. Wang, Y. Gao, Y. Long, Thermochromic VO_2 for Energy-Efficient Smart Windows, Joule. 2 (2018) 1707–1746. doi:10.1016/j.joule.2018.06.018.

[6] T.C. Chang, X. Cao, S.H. Bao, S.D. Ji, H.J. Luo, P. Jin, Review on thermochromic vanadium dioxide based smart coatings: from lab to commercial application, Adv. Manuf. 6 (2018) 1–19. doi:10.1007/s40436-017-0209-2.

[7] N. Shen, S. Chen, R. Huang, J. Huang, J. Li, R. Shi, S. Niu, A. Amini, C. Cheng, Vanadium dioxide for thermochromic smart windows in ambient conditions, Mater. Today Energy. 21 (2021) 100827. doi:10.1016/j.mtener.2021.100827.

[8] X. Cao, T. Chang, Z. Shao, F. Xu, H. Luo, P. Jin, Challenges and Opportunities toward Real Application of VO_2-Based Smart Glazing, Matter. 2 (2020) 862–881. doi:10.1016/j.matt.2020.02.009.

[9] X. Gao, C.M.M. Rosário, H. Hilgenkamp, Multi-level operation in VO_2-based resistive switching devices, AIP Adv. 12 (2022) 015218. doi:10.1063/5.0077160.

[10] G. Liu, S. Wang, A.I.Y. Tok, T.J. White, C. Li, M. Layani, S. Magdassi, M. Li, Y. Long, Self-Assembled VO_2 Mesh Film-Based Resistance Switches with High Transparency and Abrupt ON/OFF Ratio, ACS Omega. 4 (2019) 19635–19640. doi:10.1021/acsomega.9b02239.

[11] A. Simo, B. Mwakikunga, B.T. Sone, B. Julies, R. Madjoe, M. Maaza, VO_2 nanostructures based chemiresistors for low power energy consumption hydrogen sensing, Int. J. Hydrogen Energy. 39 (2014) 8147–8157. doi:10.1016/j.ijhydene.2014.03.037.

[12] J.W. Byon, M. Bin Kim, M.H. Kim, S.Y. Kim, S.H. Lee, B.C. Lee, J.M. Baik, Electrothermally induced highly responsive and highly selective vanadium oxide hydrogen sensor based on metal-insulator transition, J. Phys. Chem. C. 116 (2012) 226–230. doi:10.1021/jp2080989.

[13] A.J. Santos, M. Escanciano, A. Suárez-Llorens, M. Pilar Yeste, F.M. Morales, A Novel Route for the Easy Production of Thermochromic VO_2 Nanoparticles, Chem. - A Eur. J. 27 (2021) 16662–16669. doi:10.1002/chem.202102566.

[14] Z. Qu, L. Yao, Y. Zhang, B. Jin, J. He, J. Mi, Surface and interface engineering for VO_2 coatings with excellent optical performance: From theory to practice, Mater. Res. Bull. 109 (2019) 195–212. doi:10.1016/j.materresbull.2018.09.043.

[15] K. Liu, S. Lee, S. Yang, O. Delaire, J. Wu, Recent progresses on physics and applications of vanadium dioxide, Mater. Today. 21 (2018) 875–896. doi:10.1016/j.mattod.2018.03.029.

[16] Y. Zhang, W. Xiong, W. Chen, Y. Zheng, Recent progress on vanadium dioxide nanostructures and devices: Fabrication, properties, applications and perspectives, Nanomaterials. 11 (2021) 338. doi:10.3390/nano11020338.

[17] C. Zhao, S. Ma, Z. Li, W. Li, J. Li, Q. Hou, Y. Xing, Simple and fast fabrication of single crystal VO_2 microtube arrays, Commun. Mater. 1 (2020) 28. doi:10.1038/s43246-020-0031-4.

[18] F.M. Morales, M. Escanciano, M. P. Yeste , A. J. Santos, Reactivity of vanadium nanoparticles with oxygen and tungsten, Nanomaterials. 12 (2022) 1471. doi.org/10.3390/nano12091471.

[19] Y. Gao, H. Luo, Z. Zhang, L. Kang, Z. Chen, J. Du, M. Kanehira, C. Cao, Nanoceramic VO_2 thermochromic smart glass: A review on progress in solution processing, Nano Energy. 1 (2012) 221–246. doi:10.1016/j.nanoen.2011.12.002.

[20] J. Outón, E. Blanco, M. Domínguez, H. Bakkali, J.M. Gonzalez-Leal, J.J. Delgado, M. Ramírez-del-Solar, Tracking the optical constants of porous vanadium dioxide thin films during metal–insulator transition: Influence of processing conditions on their application in smart glasses, Appl. Surf. Sci. 580 (2022) 152228. doi:10.1016/j.apsusc.2021.152228.

[21] L. V. Yakovkina, S. V. Mutilin, V.Y. Prinz, T.P. Smirnova, V.R. Shayapov, I. V. Korol'kov, E.A. Maksimovsky, N.D. Volchok, MOCVD growth and characterization of vanadium dioxide films, J. Mater. Sci. 52 (2017) 4061–4069.

doi:10.1007/s10853-016-0669-y.

[22] H. Zhang, Z. Wu, D. Yan, X. Xu, Y. Jiang, Tunable hysteresis in metal-insulator transition of nanostructured vanadium oxide thin films deposited by reactive direct current magnetron sputtering, Thin Solid Films. 552 (2014) 218–224. doi:10.1016/j.tsf.2013.12.007.

[23] L. Kang, Y. Gao, H. Luo, Z. Chen, J. Du, Z. Zhang, Nanoporous thermochromic VO_2 films with low optical constants, enhanced luminous transmittance and thermochromic properties, ACS Appl. Mater. Interfaces. 3 (2011) 135–138. doi:10.1021/am1011172.

[24] D. Bhardwaj, A. Goswami, A.M. Umarji, Synthesis of phase pure vanadium dioxide (VO_2) thin film by reactive pulsed laser deposition, J. Appl. Phys. 124 (2018) 135301. doi:10.1063/1.5046455.

[25] J. Rezek, J. Szelwicka, J. Vlček, R. Čerstvý, J. Houška, M. Fahland, J. Fahlteich, Transfer of the sputter technique for deposition of strongly thermochromic VO_2-based coatings on ultrathin flexible glass to large-scale roll-to-roll device, Surf. Coat. Technol. 442 (2022) 128273. doi:10.1016/j.surfcoat.2022.128273.

[26] Z. Chen, Y. Tang, A. Ji, L. Zhang, Y. Gao, Large-ccale preparation of durable VO_2 nanocomposite coatings, ACS Appl. Nano Mater. 4 (2021) 4048–4054. doi:10.1021/acsanm.1c00387.

[27] Y. Kim, S. Yu, J. Park, D. Yoon, A.M. Dayaghi, K.J. Kim, J.S. Ahn, J. Son, High-throughput roll-to-roll fabrication of flexible thermochromic coatings for smart windows with VO_2 nanoparticles, J. Mater. Chem. C. 6 (2018) 3451–3458.

doi:10.1039/c7tc05876d.

[28] Y.X. Ji, G.A. Niklasson, C.G. Granqvist, M. Boman, Thermochromic VO_2 films by thermal oxidation of vanadium in SO_2, Sol. Energy Mater. Sol. Cells. 144 (2016) 713–716. doi:10.1016/j.solmat.2015.10.012.

[29] G. Rampelberg, B. De Schutter, W. Devulder, K. Martens, I. Radu, C. Detavernier, In situ X-ray diffraction study of the controlled oxidation and reduction in the V-O system for the synthesis of VO_2 and V_2O_3 thin films, J. Mater. Chem. C. 3 (2015) 11357–11365. doi:10.1039/c5tc02553b.

[30] J. Liang, X. Yu, Y. Zhao, X. Fan, W. Wu, S. Wang, Enhancement of metal-insulator transition performance of VO_2 thin films by conventional furnace annealing, Thin Solid Films. 730 (2021) 138709. doi:10.1016/j.tsf.2021.138709.

[31] L. Pósa, G. Molnár, B. Kalas, Z. Baji, Z. Czigány, P. Petrik, J. Volk, A rational fabrication method for low switching-temperature VO_2, Nanomaterials. 11 (2021) 212. doi:10.3390/nano11010212.

[32] S. Yu, S. Wang, M. Lu, L. Zuo, A metal-insulator transition study of VO_2 thin films grown on sapphire substrates, J. Appl. Phys. 122 (2017) 235102. doi:10.1063/1.4997437.

[33] A.J. Santos, B. Lacroix, M. Domínguez, R. García, N. Martin, F.M. Morales, Controlled grain-size thermochromic VO_2 coatings by the fast oxidation of sputtered vanadium or vanadium oxide films deposited at glancing angles, Surf. Interfaces. 27 (2021) 101581. doi:10.1016/j.surfin.2021.101581.

[34] S.Y. Li, G.A. Niklasson, C.G. Granqvist, Thermochromic fenestration with VO_2-

based materials: Three challenges and how they can be met, Thin Solid Films. 520 (2012) 3823–3828. doi:10.1016/j.tsf.2011.10.053.

[35] S. Dou, J. Zhao, W. Zhang, H. Zhao, F. Ren, L. Zhang, X. Chen, Y. Zhan, Y. Li, A universal approach to achieve high luminous transmittance and solar modulating ability simultaneously for vanadium dioxide smart coatings via double-sided localized surface plasmon resonances, ACS Appl. Mater. Interfaces. 12 (2020) 7302–7309. doi:10.1021/acsami.9b17923.

[36] Y. Ke, T. Wang, N. Li, S. Wang, Y. Long, On-off near-infrared absorbance based on thermal-responsive plasmonic coupling in vanadium dioxide arrays for thermochromic windows, Opt. Express. 29 (2021) 9324. doi:10.1364/oe.419872.

[37] J. Outón, A. Casas-Acuña, M. Domínguez, E. Blanco, J.J. Delgado, M. Ramírez-del-Solar, Novel laser texturing of W-doped VO_2 thin film for the improvement of luminous transmittance in smart windows application, Appl. Surf. Sci. 608 (2023) 155180. doi:10.1016/j.apsusc.2022.155180.

[38] V. Collado, N. Martin, P. Pedrosa, J.Y. Rauch, M. Horakova, M.A.P. Yazdi, A. Billard, Temperature dependence of electrical resistivity in oxidized vanadium films grown by the GLAD technique, Surf. Coat. Technol. 304 (2016) 476–485. doi:10.1016/j.surfcoat.2016.07.057.

[39] D.P. Zhang, M.D. Zhu, Y. Liu, K. Yang, G.X. Liang, Z.H. Zheng, X.M. Cai, P. Fan, High performance VO_2 thin films growth by DC magnetron sputtering at low temperature for smart energy efficient window application, J. Alloys Compd. 659 (2016) 198–202. doi:10.1016/j.jallcom.2015.11.047.

[40] F. Maudet, B. Lacroix, A.J. Santos, F. Paumier, M. Paraillous, S. Hurand, A.

Corvisier, C. Marsal, B. Giroire, C. Dupeyrat, R. García, F.M. Morales, T. Girardeau, Optical and nanostructural insights of oblique angle deposited layers applied for photonic coatings, Appl. Surf. Sci. 520 (2020) 146312. doi:10.1016/j.apsusc.2020.146312.

[41] M.M. Hawkeye, M.J. Brett, Glancing angle deposition: Fabrication, properties, and applications of micro- and nanostructured thin films, J. Vac. Sci. Technol. A Vacuum, Surfaces, Film. 25 (2007) 1317. doi:10.1116/1.2764082.

[42] A. Barranco, A. Borras, A.R. Gonzalez-Elipe, A. Palmero, Perspectives on oblique angle deposition of thin films: From fundamentals to devices, Prog. Mater. Sci. 76 (2016) 59–153. doi:10.1016/j.pmatsci.2015.06.003.

[43] C.G. Granqvist, Electrochromics and Thermochromics: Towards a New Paradigm for Energy Efficient Buildings, Mater. Today Proc. 3 (2016) S2–S11. doi:10.1016/j.matpr.2016.01.002.

[44] P.L. Madhuri, S. Bhupathi, S. Shuddhodana, Z.M.A. Judeh, S.-H. Yang, Y. Long, I. Abdulhalim, Hybrid vanadium dioxide-liquid crystal tunable non-reciprocal scattering metamaterial smart window for visible and infrared radiation control, Opt. Mater. Express. 11 (2021) 3023. doi:10.1364/ome.432784.

[45] T. Kang, Z. Ma, J. Qin, Z. Peng, W. Yang, T. Huang, S. Xian, S. Xia, W. Yan, Y. Yang, Z. Sheng, J. Shen, C. Li, L. Deng, L. Bi, Large-scale, power-efficient Au/VO_2 active metasurfaces for ultrafast optical modulation, Nanophotonics. 10 (2020) 909–918. doi:10.1515/nanoph-2020-0354.

[46] C. Batista, R.M. Ribeiro, V. Teixeira, Synthesis and characterization of VO_2-based thermochromic thin films for energy-efficient windows, Nanoscale Res.

Lett. 6 (2011) 301. doi:10.1186/1556-276X-6-301.

[47] X. Chen, M. Wu, X. Liu, D. Wang, F. Liu, Y. Chen, F. Yi, W. Huang, S. Wang, Tuning the Doping Ratio and Phase Transition Temperature of VO_2 Thin Film by Dual-Target Co-Sputtering, Nanomaterials. 9 (2019) 834. doi:10.3390/nano9060834.

[48] T. Chang, X. Cao, N. Li, S. Long, Y. Zhu, J. Huang, H. Luo, P. Jin, Mitigating Deterioration of Vanadium Dioxide Thermochromic Films by Interfacial Encapsulation, Matter. 1 (2019) 734–744. doi:10.1016/j.matt.2019.04.004.

[49] M.G. Krishna, A.K. Bhattacharya, Optical and structural properties of bias sputtered vanadium pentoxide thin films, Vacuum. 48 (1997) 879–882. doi:10.1016/s0042-207x(97)00123-1.

[50] G. Sun, X. Cao, S. Long, R. Li, P. Jin, Optical and electrical performance of thermochromic V_2O_3 thin film fabricated by magnetron sputtering, Appl. Phys. Lett. 111 (2017) 053901. doi:10.1063/1.4997323.

[51] Y.-B. Kang, Critical Evaluation and Thermodynamic Optimization of the VO–$VO_{2.5}$ System, J. Eur. Ceram. Soc. 32 (2012) 3187–3198. doi:10.1007/s11663-020-01939-0.

[52] P. Shvets, O. Dikaya, K. Maksimova, A. Goikhman, A review of Raman spectroscopy of vanadium oxides, J. Raman Spectrosc. 50 (2019) 1226–1244. doi:10.1002/jrs.5616.

[53] C. Sol, M. Portnoi, T. Li, K.L. Gurunatha, J. Schläfer, S. Guldin, I.P. Parkin, I. Papakonstantinou, High-Performance Planar Thin Film Thermochromic Window

via Dynamic Optical Impedance Matching, ACS Appl. Mater. Interfaces. 12 (2020) 8140–8145. doi:10.1021/acsami.9b18920.

[54] J. Jin, D. Zhang, X. Qin, Y. Yang, Y. Huang, H. Guan, Q. He, P. Fan, W. Lv, Notable enhancement of phase transition performance and luminous transmittance in VO_2 films via simple method of Ar/O plasma post-treatment, Nanomaterials. 9 (2019) 102. doi:10.3390/nano9010102.

[55] M. Zhou, J. Bao, M. Tao, R. Zhu, Y. Lin, X. Zhang, Y. Xie, Periodic porous thermochromic VO_2(M) films with enhanced visible transmittance, Chem. Commun. 49 (2013) 6021–6023. doi:10.1039/c3cc42112k.

[56] X. Cao, N. Wang, J.Y. Law, S.C.J. Loo, S. Magdassi, Y. Long, Nanoporous thermochromic VO_2(M) thin films: Controlled porosity, largely enhanced luminous transmittance and solar modulating ability, Langmuir. 30 (2014) 1710–1715. doi:10.1021/la404666n.

[57] M. Currie, V.D. Wheeler, B. Downey, N. Nepal, S.B. Qadri, J.A. Wollmershauser, J. Avila, L. Nyakiti, Asymmetric hysteresis in vanadium dioxide thin films, Opt. Mater. Express. 9 (2019) 3717. doi:10.1364/ome.9.003717.

[58] K.L. Gurunatha, S. Sathasivam, J. Li, M. Portnoi, I.P. Parkin, I. Papakonstantinou, Combined Effect of Temperature Induced Strain and Oxygen Vacancy on Metal-Insulator Transition of VO_2 Colloidal Particles, Adv. Funct. Mater. 30 (2020) 27–31. doi:10.1002/adfm.202005311.

[59] L. Chen, X. Wang, D. Wan, Y. Cui, B. Liu, S. Shi, H. Luo, Y. Gao, Tuning the

phase transition temperature, electrical and optical properties of VO_2 by oxygen nonstoichiometry: Insights from first-principles calculations, RSC Adv. 6 (2016) 73070–73082. doi:10.1039/c6ra09449j.

[60] G. Xu, P. Jin, M. Tazawa, K. Yoshimura, Thickness dependence of optical properties of VO_2 thin films epitaxially grown on sapphire (0001), Appl. Surf. Sci. 244 (2005) 449–452. doi:10.1016/j.apsusc.2004.09.157.

[61] X. Zhou, Y. Meng, T.D. Vu, D. Gu, Y. Jiang, Q. Mu, Y. Li, B. Yao, Z. Dong, Q. Liu, Y. Long, A new strategy of nanocompositing vanadium dioxide with excellent durability, J. Mater. Chem. A. 9 (2021) 15618–15628. doi:10.1039/d1ta02525b.

[62] J. Bian, M. Wang, H. Sun, H. Liu, X. Li, Y. Luo, Thickness-modulated metal–insulator transition of VO_2 film grown on sapphire substrate by MBE, J. Mater. Sci. 51 (2016) 6149–6155. doi:10.1007/s10853-016-9863-1.

[63] T.D. Vu, H. Xie, S. Wang, J. Hu, X. Zeng, Y. Long, Durable vanadium dioxide with 33-year service life for smart windows applications, Mater. Today Energy. 26 (2022) 100978. doi:10.1016/j.mtener.2022.100978.

[64] W. Li, S. Ji, Y. Li, A. Huang, H. Luo, P. Jin, Synthesis of VO_2 nanoparticles by a hydrothermal-assisted homogeneous precipitation approach for thermochromic applications, RSC Adv. 4 (2014) 13026–13033. doi:10.1039/c3ra47666a.

[65] M. Benkahoul, M.K. Zayed, A. Solieman, S.N. Alamri, Spray deposition of V_4O_9 and V_2O_5 thin films and post-annealing formation of thermochromic VO_2, J. Alloys Compd. 704 (2017) 760–768. doi:10.1016/j.jallcom.2017.02.088.

[66] A.J. Santos, N. Martin, J. Outón, A. Casas-Acuña, E. Blanco, R. García, F.M. Morales, Atmospheric flash annealing of low-dimensional vanadium nanolayers sputtered on glass substrates, Surf. Interfaces. 34 (2022) 102313. doi:10.1016/j.surfin.2022.102313.

[67] I.H. Hwang, Y. Park, J.M. Choi, S.W. Han, Direct comparison of the electrical, optical, and structural phase transitions of VO_2 on ZnO nanostructures, Curr. Appl. Phys. 36 (2022) 1–8. doi:10.1016/j.cap.2021.12.016.

GRAPHICAL ABSTRACT